The Astrophysical Journal, 720:1038–1044, 2010 September 10 doi:10.1088/0004-637X/720/2/1038

AN ANALYTIC MODEL OF THE PHYSICAL PROPERTIES OF GALAXY CLUSTERS

G. Esra Bulbul[1], Nicole Hasler[1], Massimiliano Bonamente[1,2], and Marshall Joy[2]
[1] Department of Physics, University of Alabama, Huntsville, AL 35899, USA
[2] Space Science Office, VP62, NASA Marshall Space Flight Center, Huntsville, AL 35812, USA
Received 2009 November 16; accepted 2010 April 27; published 2010 August 17

ABSTRACT

We introduce an analytic model of the diffuse intergalactic medium in galaxy clusters based on a polytropic equation of state for the gas in hydrostatic equilibrium with the cluster gravitational potential. This model is directly applicable to the analysis of X-ray and Sunyaev–Zel'dovich effect observations from the cluster core to the virial radius, with five global parameters and three parameters describing the cluster core. We validate the model using *Chandra* X-ray observations of two polytropic clusters, MS 1137.5+6625 and CL J1226.9+3332, and two cool core clusters, 1835 and A2204. We show that the model accurately describes the spatially resolved spectroscopic and imaging data, including the cluster core region where significant cooling of the plasma is observed.

Key words: galaxies: individual (Abell 1835, Abell 2204) – X-rays: galaxies: clusters

Online-only material: color figures

1. INTRODUCTION

Galaxy cluster masses play an important role in addressing fundamental physical and cosmological problems, such as the measurement of the cluster gas mass fraction (Allen et al. 2008; Ettori et al. 2009), the evolution of the growth of structure (Mantz et al. 2008, 2009; Vikhlinin et al. 2009), and the gravitational sedimentation of ions (Chuzhoy & Nusser 2003; Peng & Nagai 2009; Shtykovskiy & Gilfanov 2010). A vital tool for the measurement of cluster masses is the diffuse hot intergalactic medium which can be detected primarily through its bright X-ray emission (Sarazin 1988), or through the Sunyaev–Zel'dovich effect (SZE; Sunyaev & Zel'dovich 1972; Carlstrom et al. 2002). A variety of models are used to describe the distribution of the gas, from the simple isothermal β model (Cavaliere & Fusco-Femiano 1976; Birkinshaw et al. 1991) to more complex models that describe either the X-ray properties (gas density and temperature; Vikhlinin et al. 2006; Cavaliere et al. 2009) or the SZE properties (gas pressure; Nagai et al. 2007; Mroczkowski et al. 2009; Arnaud et al. 2009).

We investigate a model of galaxy clusters based on an analytic distribution for the cluster mass density inspired by the Navarro et al. (1996) distribution, which we generalize following Suto et al. (1998), Ascasibar et al. (2003), and Ascasibar & Diego (2008) to include a variable asymptotic slope at large radii. This mass density is combined with a polytropic equation of state for the gas, to provide self-consistent density, temperature, and pressure profiles for a plasma in hydrostatic equilibrium. The use of a polytropic equation of state for the cluster gas has also been recently proposed by Ascasibar & Diego (2008) and Bode et al. (2009) and tested observationally by Sanderson & Ponman (2010).

In this paper, we derive analytic radial profiles for the physical quantities (temperature, density, and pressure) relevant to X-ray and SZE observations and present an application of these models to high-resolution *Chandra* observations of the galaxy clusters MS 1137.5+6625, CL J1226.9+3332, A1835, and A2204. Applications of this new model include measurement of gas mass fraction from joint X-ray and SZE observations (N. Hasler et al. 2010, in preparation) and the effect of He sedimentation on X-ray mass estimates (G. E. Bulbul et al. 2010, in preparation). This paper is organized as follows: in Section 2, we describe our model; in Section 3, we present the application of the model to *Chandra* X-ray observations of MS 1137.5+6625, CL J1226.9+3332, A2204, and A1835; and in Section 4, we perform a comparison between our mass measurements and the results of Mroczkowski et al. (2009). In Section 5, we present our conclusions. In the analysis of the *Chandra* data, we assume the cosmological parameters $h = 0.73$, $\Omega_M = 0.27$, and $\Omega_\Lambda = 0.73$.

2. A MODEL OF THE INTERGALACTIC MEDIUM BASED ON HYDROSTATIC EQUILIBRIUM AND THE POLYTROPIC EQUATION OF STATE

2.1. The Mass Density Distribution

The cluster gravitational potential is dominated by dark matter, with the intergalactic medium and stars contributing less than approximately ∼20% of the mass (Allen et al. 2004, 2008; Ettori et al. 2009; Vikhlinin et al. 2009). We therefore start with a total mass density distribution that is obtained as a generalization of the Navarro et al. (1996) profile:

$$\rho_{\rm tot}(r) = \frac{\rho_i}{(r/r_s)(1+r/r_s)^\beta}, \quad (1)$$

where ρ_i is the normalization constant, r_s is a characteristic scale radius, and β+1 is the slope of the density distribution at large radii. Equation (1) is a simplified version of the density distribution introduced by Suto et al. (1998).

The total mass enclosed within radius r can be found by taking the volume integral of the density (Equation (1)):

$$M(r) = \frac{4\pi\rho_i r_s^3}{(\beta-2)}\left(\frac{1}{\beta-1} + \frac{1/(1-\beta) - r/r_s}{(1+r/r_s)^{\beta-1}}\right). \quad (2)$$

Equation (2) is indeterminate at $\beta = 2$; the limit at $\beta = 2$ can be determined using L'Hospital's rule:

$$M(r) = 4\pi\rho_i r_s^3\left(\ln(1+r/r_s) - \frac{r/r_s}{1+r/r_s}\right) \quad [\beta = 2], \quad (3)$$

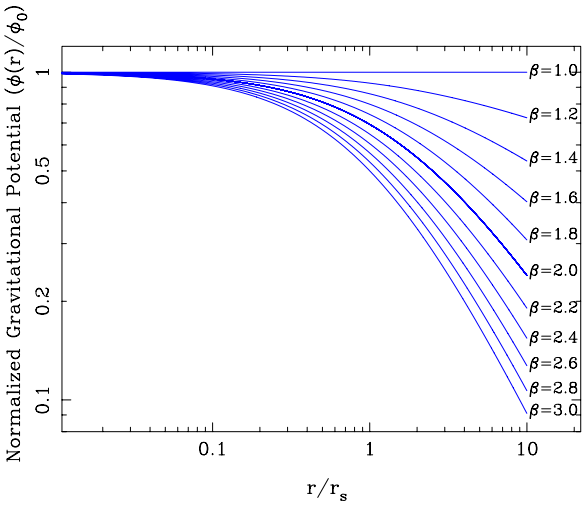

Figure 1. Normalized gravitational potential for various values of the β parameter.

(A color version of this figure is available in the online journal.)

and therefore the mass is a continuous function of β with no discontinuity at $\beta = 2$.

The gravitational potential at a distance r is found by

$$d\phi(r) = GM(r)/r^2 dr \tag{4}$$

using the boundary condition $\phi(\infty) = 0$. Equation (4) can be integrated analytically

$$\phi(r) = \phi_0 \left(\frac{1}{(\beta - 2)} \frac{(1 + r/r_s)^{\beta-2} - 1}{r/r_s (1 + r/r_s)^{\beta-2}} \right), \tag{5}$$

where

$$\phi_0 = -\frac{4\pi G \rho_i r_s^2}{(\beta - 1)}. \tag{6}$$

The potential at $\beta = 2$ is also found by using L'Hospital's rule,

$$\phi(r) = \phi_0 \left(\frac{\ln(1 + r/r_s)}{r/r_s} \right) \quad [\beta = 2]. \tag{7}$$

Therefore, the gravitational potential is a continuous function of β with no discontinuity at $\beta = 2$. Figure 1 shows the radial distribution of the gravitational potential for $1.0 \leqslant \beta \leqslant 3.0$. The limiting value of $\beta = 1$ is shown in Figure 1 corresponding to a constant potential.

2.2. Gas Density and Temperature Profile

The diffuse gas is assumed to be in hydrostatic equilibrium with the gravitational potential. Assuming spherical symmetry,

$$\frac{1}{\mu m_p n_e(r)} \frac{dP_e}{dr} = -\frac{d\phi(r)}{dr}, \tag{8}$$

where $P_e(r) = n_e(r) kT(r)$ is the electron pressure, G denotes the gravitational constant, m_p is the proton mass, μ is the mean molecular weight of the plasma, k is the Boltzmann constant, and $n_e(r)$ is the electron number density. In order to solve Equation (8), we assume that the gas follows a polytropic equation of state,

$$\frac{n_{e,\mathrm{poly}}(r)}{n_{e0}} = \left[\frac{T_{\mathrm{poly}}(r)}{T_0} \right]^n, \tag{9}$$

where n is the polytropic index, and n_{e0} and T_0 are the values of the number density and temperature, respectively, at $r = 0$. The polytropic index $n > 0$ is a free parameter of the model, with the limit $n \to \infty$ describing an isothermal distribution of gas (Eddington 1926).

The temperature profile is obtained as a function of the gravitational potential from Equations (8) and (9),

$$T_{\mathrm{poly}}(r) = -\frac{1}{(n+1)} \frac{\mu m_p}{k} \phi(r), \tag{10}$$

and therefore, using Equation (5),

$$T_{\mathrm{poly}}(r) = T_0 \left(\frac{1}{(\beta - 2)} \frac{(1 + r/r_s)^{\beta-2} - 1}{r/r_s (1 + r/r_s)^{\beta-2}} \right), \tag{11}$$

where the normalization constant T_0 is obtained from Equations (6) and (10):

$$T_0 = \frac{4\pi G \mu m_p}{k(n+1)} \frac{r_s^2 \rho_i}{(\beta - 1)}. \tag{12}$$

Equation (10) shows that $T_{\mathrm{poly}}(r) \propto \phi(r)$, and therefore Figure 1 also describes $T_{\mathrm{poly}}(r)$ as a function of radius. Equation (12) links the gas temperature to the normalization of the matter density ρ_i, and therefore, the depth of the gravitational potential can be determined from the observed temperature profile.

Using the relation between temperature and gas density provided by the polytropic relation (Equation (9)), the polytropic gas density profile is

$$n_{e,\mathrm{poly}}(r) = n_{e0} \left(\frac{1}{(\beta - 2)} \frac{(1 + r/r_s)^{\beta-2} - 1}{r/r_s (1 + r/r_s)^{\beta-2}} \right)^n. \tag{13}$$

2.3. The Electron Gas Pressure

The gas pressure is obtained using the ideal gas law $P_e(r) = n_{e,\mathrm{poly}}(r) k T_{\mathrm{poly}}(r)$,

$$P_e(r) = P_{e0} \left(\frac{1}{(\beta - 2)} \frac{(1 + r/r_s)^{\beta-2} - 1}{r/r_s (1 + r/r_s)^{\beta-2}} \right)^{n+1}. \tag{14}$$

In the limit $\beta \to 2$, the pressure is analytically described by

$$P_e(r) = P_{e0} \left(\frac{\ln(1 + r/r_s)}{r/r_s} \right)^{n+1} \quad [\beta = 2]. \tag{15}$$

The electron pressure for this model has only four free parameters, and it is suitable for the analysis of SZE observations of galaxy clusters (N. Hasler et al. 2010, in preparation).

2.4. Cool Core Clusters

Although the temperature profile predicted by the polytropic model provides a good description at intermediate to large radii, cool core clusters feature a significant temperature drop in the central region which cannot be approximated by a polytropic equation of state (see, for example, Vikhlinin et al. 2005, 2006; Sanderson et al. 2006; Baldi et al. 2007). For cool core clusters, we introduce a modified temperature profile

$$T(r) = T_{\mathrm{poly}}(r) \tau_{\mathrm{poly}}(r), \tag{16}$$

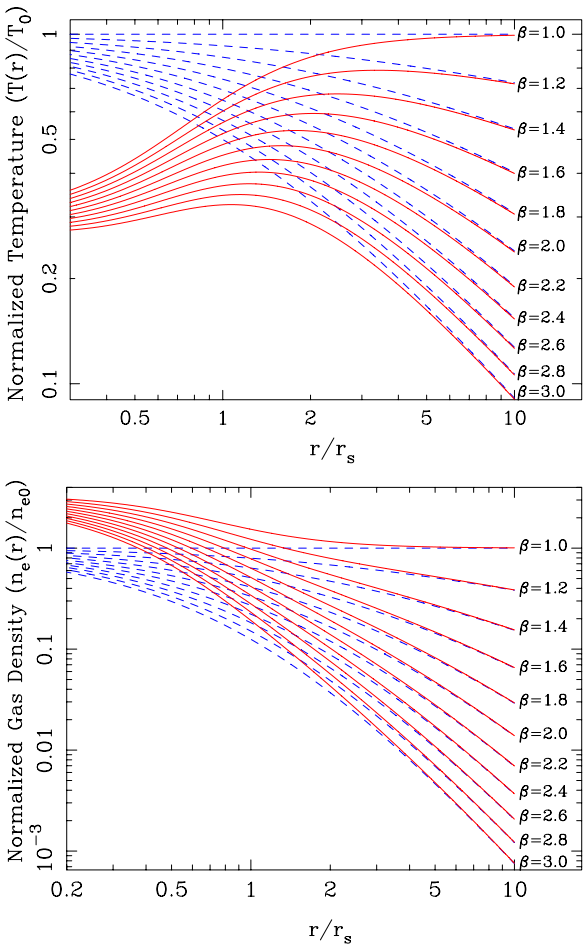

Figure 2. Solid red lines are the normalized temperature and density profiles for a taper function with parameters $\alpha = 0.3$, $r_{\rm cool} = r_s$, and $\gamma = 2.0$, and variable values for β; blue dashed lines are the models without the core taper function.
(A color version of this figure is available in the online journal.)

where $T_{\rm poly}(r)$ is the temperature profile according to the polytropic equation of state (Equation (11)) and $\tau_{\rm cool}(r)$ is a phenomenological core taper function used by Vikhlinin et al. (2006):

$$\tau_{\rm cool}(r) = \frac{\alpha + (r/r_{\rm cool})^{\gamma}}{1 + (r/r_{\rm cool})^{\gamma}}, \quad (17)$$

where $0 < \alpha < 1$ is a free parameter that measures the amount of central cooling, and $r_{\rm cool}$ is a characteristic cooling radius. The temperature profile modified by the core taper function is shown in Figure 2 for representative values of parameters $r_{\rm cool}$, γ, and α.

Therefore, the explicit temperature profile for cool core clusters is given by

$$T(r) = T_0 \left(\frac{1}{(\beta - 2)} \frac{(1 + r/r_s)^{\beta-2} - 1}{r/r_s (1 + r/r_s)^{\beta-2}} \right) \tau_{\rm cool}(r). \quad (18)$$

In order to calculate the density distribution for cool core clusters, we assume that the pressure distribution is the same as in the polytropic case (Equation (14)). Therefore, the electron density is given by

$$n_e(r) = \frac{P_e(r)}{kT(r)} = n_{e0} \left(\frac{1}{(\beta - 2)} \frac{(1 + r/r_s)^{\beta-2} - 1}{r/r_s (1 + r/r_s)^{\beta-2}} \right)^{n} \tau_{\rm cool}^{-1}(r). \quad (19)$$

Table 1
Cluster Sample

Cluster	z	N_H[a] ($\rm cm^{-2}$)	Obs. ID	Exposure Time (ks)
A2204	0.152[b]	5.67×10^{20}	7940	72.9
A1835	0.252[b]	2.04×10^{20}	6880	110.0
MS 1137.5+6625	0.784[c]	9.54×10^{19}	536	115.5
CL J1226.9+3332	0.888[d]	1.38×10^{20}	5014	32.7
			3180	31.5

Notes.
[a] Leiden/Argentine/Bonn (LAB) Survey, see Kalberla et al. (2005).
[b] Struble & Rood (1999).
[c] Donahue et al. (1999).
[d] Ebeling et al. (2001).

The behavior of the gas density for various core taper parameters is shown in Figure 2.

For hydrostatic equilibrium to be satisfied, these modified density and temperature distributions require a modified total mass distribution:

$$M(r) = \frac{4\pi \rho_i r_s^3}{(\beta - 2)} \left(\frac{1}{\beta - 1} + \frac{1/(1 - \beta) - r/r_s}{(1 + r/r_s)^{\beta-1}} \right) \tau_{\rm cool}(r). \quad (20)$$

The only difference between the cool core total mass distribution (Equation (20)) and the polytropic total mass distribution (Equation (2)) is the term $\tau_{\rm cool}(r)$, which is significant only at small radii. At large radii, the effect of the core taper vanishes, and the thermodynamics of the gas is described by the polytropic equation of state.

3. APPLICATION TO *CHANDRA* OBSERVATIONS OF CLUSTERS

3.1. Chandra Data Reduction and Analysis

We use deep *Chandra* ACIS-I observations of four galaxy clusters to validate our models: two clusters which do not have a cool core component, MS 1137.5+6625 and CL J1226.9+3332, and two cool core clusters, A2204 and A1835. The observations are summarized in Table 1. As part of the data reduction procedure, we applied afterglow, bad pixel, and charge transfer inefficiency corrections to the level 1 event files using CIAO 4.1 and CALDB 4.1.1. Flares in the background due to solar activity are eliminated using light curve filtering as described in Markevitch et al. (2003). Filtered exposure times are also given in Table 1.

For the purpose of background subtraction, we use blank-sky observations. Given that the background is obtained from regions of the sky that may have different soft X-ray fluxes than at the cluster position, we use a peripheral region of the ACIS-I detector to model the difference between the blank-sky and the cluster soft fluxes. This step in the analysis is particularly important for A2204, which lies in a region of significantly higher soft X-ray emission than the average blank-sky region. Spectra and images used in this paper are extracted in the energy band 0.7–7.0 keV, chosen to minimize the effect of calibration uncertainties at the lowest energies and the effect of the detector background at high energy.

Spectra are extracted in concentric annuli surrounding the centroid of X-ray emission after all point sources were removed. An optically thin plasma emission model (APEC in XSPEC) is used, with temperature, abundance, and normalization as free

Table 2
Sources of Systematic Error in the *Chandra* Data

Source of Uncertainty	Observable Affected	Fractional Error
Background level	Background count rate	5%
Spatial variations of $A_{\rm eff}$[a]	Photon count rates	1%
Energy calibration of $A_{\rm eff}$[b]	Temperature measurement	5%

Notes.
[a] Reference: http://cxc.harvard.edu/cal/
[b] Reference: http://cxc.harvard.edu/ciao4.1/why/caldb4.1.1_hrma.html

parameters. The redshift and Galactic N_H of the four clusters are shown in Table 1.

3.2. Systematic Uncertainties in the Chandra Data Analysis

We consider possible sources of systematic uncertainty in the *Chandra* data. The blank-sky background used in our analysis is normalized to the high-energy background level of each cluster observation, determined from peripheral regions of the ACIS detector that are free of cluster emission (following Markevitch et al. 2003). The primary source of uncertainty in the background subtraction is the choice of a peripheral region as a representative of the background at the cluster location. Due to the scatter in the count rate of various peripheral regions in each cluster observation, we estimate a ∼5% uncertainty in the determination of the background level from these *Chandra* observations. We use this uncertainty in the spectral and imaging data analysis.

Calibration of the ACIS effective area is another significant source of systematic uncertainty in our analysis. For the spectral data used for measuring the gas temperature, the primary source of uncertainty is the low-energy calibration of the effective area and the presence of a contaminant on the optical filter of the ACIS detector. We use the *Chandra* calibration available in CALDB 4.1.1, which includes a significant change in the effective area calibration which improves the agreement between cluster temperatures obtained with ACIS-I and also with other instruments (such as *XMM-Newton*'s EPIC). With this calibration of the *Chandra* efficiency, we estimate that any residual systematic error in the measurement of cluster temperatures is of the order ∼5% and add this error to the temperature measured in each bin.

For the imaging data, spatially dependent non-uniformities in the ACIS efficiency are a relevant source of possible systematic error because of the extended nature of the sources. The absolute calibration of the ACIS efficiency is currently at the level of 3%, with possible spatial variations on arcmin scales at the level of ∼1%; we use a 1% error as an additional uncertainty in the count rates for each annulus.

Table 2 provides a summary of the uncertainties included in our analysis of the *Chandra* data and references to the *Chandra* calibration information.

3.3. Result of Model Fits and Mass Measurements

The radial profiles of the X-ray surface brightness and temperature observed from the *Chandra* data are used to determine the best-fit parameters and the goodness of fit for MS 1137.5+6625, CL J1226.9+3332, A1835, and A2204. The X-ray surface brightness is

$$S_x = \frac{1}{4\pi(1+z)^3}\int n_e^2 \Lambda_{ee}(T)\, dl, \qquad (21)$$

where S_x is in detector units (counts cm^{-2} arcmin^{-2} s^{-1}), z is the cluster redshift, $\Lambda_{ee}(T)$ is the plasma emissivity in detector units (counts cm^3 s^{-1}), which we calculate using the APEC code (Smith et al. 2001), and l is the distance along the line of sight.

We validate the model using two polytropic clusters which do not have a cool core component, MS 1137.5+6625 and CL J1226.9+3332, and two cool core clusters, A1835 and A2204. We use the Monte Carlo Markov Chain code described in Bonamente et al. (2004; see Figure 3) for the fit. The model described in Section 2 has eight free parameters, of which five parameters describe the global cluster properties (n_{e0}, T_{e0}, r_s, β, and n), and three additional parameters ($r_{\rm cool}$, α, and γ) are used to model the central region of the cool core clusters.

3.3.1. Polytropic Clusters MS 1137.5+6625 and CL J1226.9+3332

For polytropic clusters, which do not have a cool core component, five parameters are sufficient to describe the distribution of density and temperature. We fixed β to 2 for these clusters (Navarro et al. 1996), since both the polytropic index (n) and β cannot be determined from X-ray data available. We report the χ^2 of the best-fit model for MS 1137.5+6625 and CL J1226.9+3332 in Table 3. We also calculate the gas mass by taking the volume integral of Equation (13) and the total mass using Equation (2) and report the results in Table 4.

3.3.2. Cool Core Clusters, A2204 and A1835

The clusters A2204 and A1835 have a clear cool core component (see Figure 4), which requires the use of the cooling equations described in Section 2.4. The best-fit model parameters are listed in Table 3. We also calculate the gas mass by taking the volume integral of Equation (19) and the total mass using Equation (20) and report the results in Table 4.

4. COMPARISON WITH PREVIOUS WORK

In Table 5, we present the comparison of mass measurements of A1835 produced by the polytropic model with the masses reported in Mroczkowski et al. (2009) at r_{2500} and r_{500}. For this purpose, we calculate the gas mass and total mass at the same radii r_{2500} and r_{500} as in Mroczkowski et al. (2009), and use the same Gaussian uncertainty on r_Δ in order to have a fair

Table 3
Best-fit Parameters of the Model

Cluster	n_{e0} (10^{-2}cm^{-3})	r_s (arcsec)	n	β	T_0 (keV)	$r_{\rm cool}$ (arcsec)	α	γ	χ^2 (dof)	P value
MS 1137.5+6625	$2.17^{+0.07}_{-0.19}$	$23.84^{+10.88}_{-2.19}$	$4.83^{+1.30}_{-0.27}$	2.0	$7.84^{+1.08}_{-1.26}$	···	···	···	14.4 (26)	96.7 %
CL J1226.9+3332	$3.99^{+0.23}_{-0.23}$	$22.65^{+5.06}_{-2.79}$	$4.54^{+0.54}_{-0.31}$	2.0	$13.32^{+2.28}_{-2.98}$	···	···	···	14.6 (29)	98.8%
A2204	$4.42^{+0.37}_{-0.24}$	$21.73^{+1.50}_{-2.01}$	$6.44^{+1.02}_{-0.51}$	$1.39^{+0.04}_{-0.06}$	$14.28^{+0.75}_{-0.78}$	$19.42^{+0.60}_{-0.73}$	$0.16^{+0.01}_{-0.01}$	2.0	115.5 (145)	96.6%
A1835	$2.57^{+0.29}_{-0.07}$	$40.32^{+3.29}_{-6.48}$	$3.98^{+0.73}_{-0.41}$	$1.94^{+0.15}_{-0.22}$	$18.26^{+0.42}_{-1.61}$	$22.65^{+0.28}_{-1.17}$	$0.18^{+0.02}_{-0.01}$	2.0	99.3 (93)	30.8%

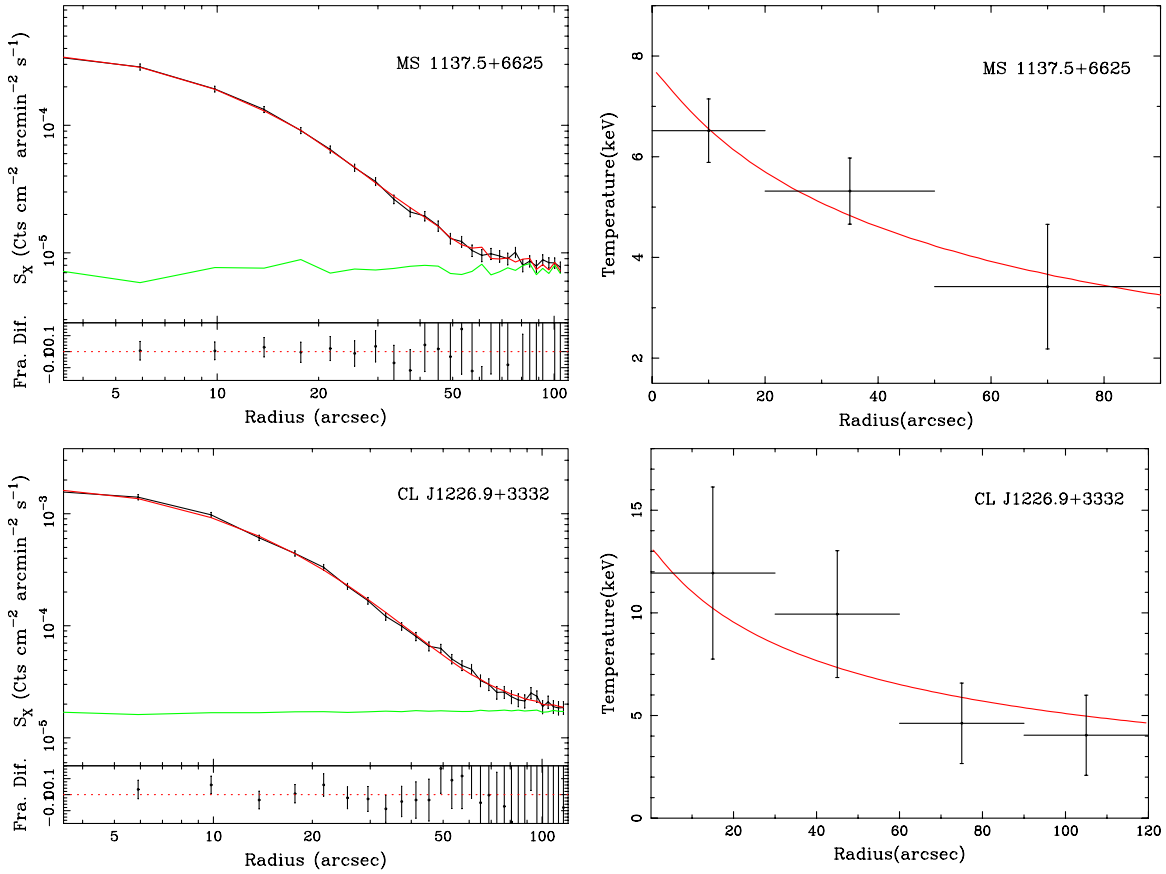

Figure 3. X-ray surface brightness and temperature profiles of MS 1137.5+6625 in the radial range 0″–90″ and CL J1226.9+3332 in the radial range 0″–120″. The red line in both profiles shows the best-fit model to the data; the green line in surface brightness profiles shows the background level. The overall χ^2 of the fit (Table 3) is the sum of the χ^2 values of the surface brightness profile and the temperature profile.

(A color version of this figure is available in the online journal.)

Table 4
Gas and Total Masses

Cluster	r_{2500} (arcsec)	$M_{\rm gas}(r_{2500})$ ($10^{13}\ M_\odot$)	$M_{\rm tot}(r_{2500})$ ($10^{14}\ M_\odot$)	r_{500} (arcsec)	$M_{\rm gas}(r_{500})$ ($10^{13}\ M_\odot$)	$M_{\rm tot}(r_{500})$ ($10^{14}\ M_\odot$)
MS 1137.5+6625	$44.7^{+4.1}_{-3.8}$	$1.10^{+0.13}_{-0.11}$	$1.20^{+0.36}_{-0.28}$	$98.5^{+9.6}_{-8.2}$	$3.08^{+0.13}_{-0.13}$	$2.56^{+0.82}_{-0.59}$
CL J1226.9+3332	$48.8^{+4.7}_{-5.3}$	$3.01^{+0.39}_{-0.44}$	$2.16^{+0.69}_{-0.63}$	$104.6^{+9.1}_{-10.4}$	$8.29^{+0.55}_{-0.63}$	$4.25^{+1.22}_{-1.14}$
A2204	$225.7^{+4.1}_{-4.1}$	$3.99^{+0.09}_{-0.09}$	$3.37^{+0.19}_{-0.18}$	$479.8^{+11.4}_{-11.2}$	$10.35^{+0.26}_{-0.26}$	$6.47^{+0.47}_{-0.44}$
A1835	$150.6^{+3.4}_{-4.2}$	$4.97^{+0.14}_{-0.17}$	$3.72^{+0.26}_{-0.30}$	$309.7^{+9.8}_{-13.1}$	$12.08^{+0.38}_{-0.50}$	$6.47^{+0.64}_{-0.79}$

comparison on masses. The gas mass measurements produced by the polytropic model are consistent with the Mroczkowski et al. (2009) results at the 1σ level (see Table 5).

The *Chandra* Calibration Database (CALDB) has recently been revised to correct the effective area, resulting in lower X-ray temperatures, especially for massive clusters.[3] The peak X-ray temperatures reported by Mroczkowski et al. (2009) using CALDB 3.4 are ∼2 keV greater than the temperatures derived in this paper using the recent calibration (CALDB 4.1.1). From Equations (2) and (20), we estimate that this temperature change would reduce the total masses reported by Mroczkowski et al. (2009) by 17% (see Table 5). When the X-ray temperature calibration issue is accounted for, the total mass values in Table 5 are in agreement with the stated 1σ uncertainties.

[3] See: http://cxc.harvard.edu/caldb/downloads/Release_notes/CALDB_v4.1.1.html.

5. DISCUSSION AND CONCLUSIONS

We introduce a new model to describe the physical properties of the hot intra-cluster medium and present an application of the model to *Chandra* X-ray observations of MS 1137.5+6625, CL J1226.9+3332, A1835, and A2204. The model is based on a polytropic equation of state for the gas in hydrostatic equilibrium with the cluster gravitational potential. Using a function for the cluster total mass density that has the asymptotic slope as a free parameter, we obtain analytic expressions for the gas density, temperature, and pressure. We also include a core taper function that accounts for the cooling of the gas in the cluster center.

This model has a number of features that make it suitable for the analysis of X-ray and SZE observations of galaxy clusters. The model is analytic and has a limited number of parameters, which describe the global properties of the cluster. For clusters which do not have a cool core, five parameters are sufficient to describe the distribution of density, temperature, pressure, and

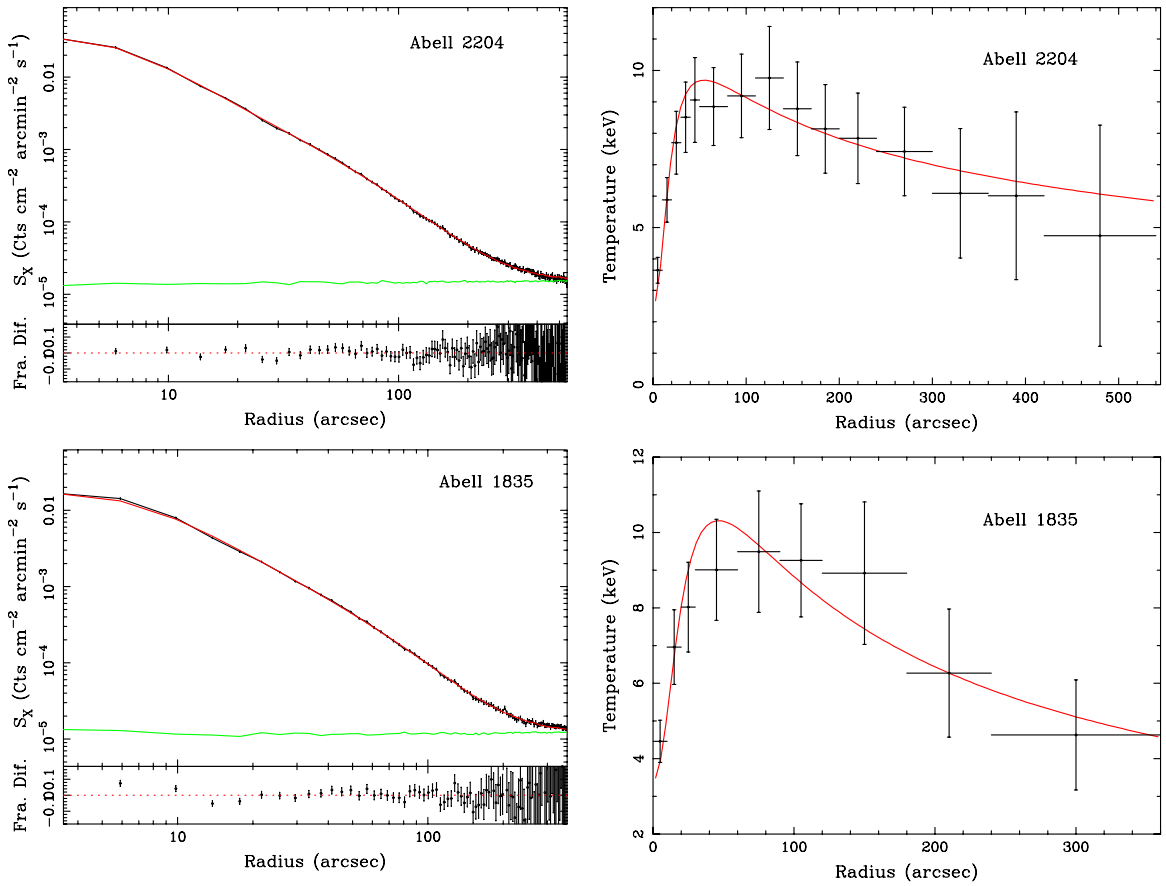

Figure 4. X-ray surface brightness and temperature profiles of cool core clusters A2204 in the radial range 0″–540″and A1835 in the radial range 0″–360″. The red line in both profiles shows the best-fit model to the data; the green line shows the background level. The overall χ^2 of the fit (Table 3) is the sum of the χ^2 values of the surface brightness profile and the temperature profile.

(A color version of this figure is available in the online journal.)

Table 5
Mass Comparison of A1835 with Mroczkowski et al. (2009)

Model	r_{2500} (arcsec)	$M_{2500,\mathrm{gas}}$ (10^{13} M_{sun})	$M_{2500,\mathrm{tot}}$ (10^{14} M_{sun})	r_{500} (arcsec)	$M_{500,\mathrm{gas}}$ (10^{13} M_{sun})	$M_{500,\mathrm{tot}}$ (10^{14} M_{sun})
A1835						
Mroczkowski et al. (2009)	$169.0^{+5.5}_{-8.0}$	$5.77^{+0.25}_{-0.35}$	$5.30^{+0.53}_{-0.72}$[a]	$363.0^{+17.0}_{-12.0}$	$13.94^{+0.64}_{-0.52}$	$10.68^{+1.54}_{-1.01}$[b]
Polytropic Model (this work)	$169.0^{+7.0}_{-7.0}$	$5.79^{+0.35}_{-0.46}$	$4.13^{+0.31}_{-0.32}$	$363.0^{+15.0}_{-15.0}$	$14.31^{+0.71}_{-0.82}$	$7.37^{+0.82}_{-0.83}$

Notes.
[a] When X-ray temperature is recalibrated using CALDB 4.1.1, mean value of $M_{2500,\mathrm{tot}}$ decreases to $\sim 4.40 \times 10^{14}$ M_{sun}.
[b] When X-ray temperature is recalibrated using CALDB 4.1.1, mean value of $M_{500,\mathrm{tot}}$ decreases to $\sim 8.86 \times 10^{14}$ M_{sun}.

total matter density. The gas density and temperature are linked by the polytropic equation of state, and the total matter density is related to the plasma properties by the hydrostatic equation. Therefore, there is just one scale radius (r_s) that appears in the radial distribution of all thermodynamic quantities. The other parameters that describe the global physical properties of the cluster are the central density (n_{e0}) and temperature (T_0) of the gas, the polytropic index n, and the asymptotic slope of the total mass density ($\beta + 1$). For cool core clusters, three additional parameters allow an accurate description of the cooling of the gas in the core and the accompanying increase in the density (Section 2.4).

In addition to the analysis of spatially resolved spectroscopic and imaging X-ray data (see Section 3), the model is applicable to SZE observations, which require a model for the plasma pressure. A number of models suitable for SZE observations are available in the literature, such as, for example, Nagai et al. (2007) and Mroczkowski et al. (2009). Our model has the advantage of the simultaneous applicability to both X-ray and SZE observations, and it is therefore suitable for a number of cosmological applications including the measurement of the Hubble constant (Bonamente et al. 2006), the measurement of scaling relations between X-ray and SZE observables (Bonamente et al. 2008), the measurement of cluster masses independent of cosmology from joint X-ray and SZE data (N. Hasler et al. 2010, in preparation), and the measurement of the effect of He sedimentation on X-ray measured masses (G. E. Bulbul et al. 2010, in preparation).

The authors thank the referee, and J. Carlstrom, D. Marrone, and T. Mroczkowski for their useful comments on the manuscript.

REFERENCES

Allen, S. W., Rapetti, D. A., Schmidt, R. W., Ebeling, H., Morris, R. G., & Fabian, A. C. 2008, MNRAS, 383, 879

Allen, S. W., Schmidt, R. W., Ebeling, H., Fabian, A. C., & van Speybroeck, L. 2004, MNRAS, 353, 457

Arnaud, M., Pratt, G. W., Piffaretti, R., Boehringer, H., Croston, J. H., & Pointecouteau, E. 2009, arXiv:0910.1234

Ascasibar, Y., & Diego, J. M. 2008, MNRAS, 383, 369

Ascasibar, Y., Yepes, G., Müller, V., & Gottlöber, S. 2003, MNRAS, 346, 731

Baldi, A., Ettori, S., Mazzotta, P., Tozzi, P., & Borgani, S. 2007, ApJ, 666, 835

Birkinshaw, M., Hughes, J. P., & Arnaud, K. A. 1991, ApJ, 379, 466

Bode, P., Ostriker, J. P., & Vikhlinin, A. 2009, ApJ, 700, 989

Bonamente, M., Joy, M. K., Carlstrom, J. E., Reese, E. D., & LaRoque, S. J. 2004, ApJ, 614, 56

Bonamente, M., Joy, M. K., LaRoque, S. J., Carlstrom, J. E., Nagai, D., & Marrone, D. P. 2008, ApJ, 675, 106

Bonamente, M., Joy, M. K., LaRoque, S. J., Carlstrom, J. E., Reese, E. D., & Dawson, K. S. 2006, ApJ, 647, 25

Carlstrom, J. E., Holder, G. P., & Reese, E. D. 2002, ARA&A, 40, 643

Cavaliere, A., & Fusco-Femiano, R. 1976, A&A, 49, 137

Cavaliere, A., Lapi, A., & Fusco-Femiano, R. 2009, ApJ, 698, 580

Chuzhoy, L., & Nusser, A. 2003, MNRAS, 342, L5

Donahue, M., Voit, G. M., Scharf, C. A., Gioia, I. M., Mullis, C. R., Hughes, J. P., & Stocke, J. T. 1999, ApJ, 527, 525

Ebeling, H., Jones, L. R., Fairley, B. W., Perlman, E., Scharf, C., & Horner, D. 2001, ApJ, 548, L23

Eddington, A. S. (ed.) 1926, The Internal Constitution of the Stars (Cambridge: Cambridge Univ. Press)

Ettori, S., Morandi, A., Tozzi, P., Balestra, I., Borgani, S., Rosati, P., Lovisari, L., & Terenziani, F. 2009, A&A, 501, 61

Kalberla, P. M. W., Burton, W. B., Hartmann, D., Arnal, E. M., Bajaja, E., Morras, R., & Poumlppel, W. G. L. 2005, A&A, 440, 775

Mantz, A., Allen, S. W., Ebeling, H., & Rapetti, D. 2008, MNRAS, 387, 1179

Mantz, A., Allen, S. W., Rapetti, D., & Ebeling, H. 2009, arXiv:0909.3098

Markevitch, M., et al. 2003, ApJ, 583, 70

Maughan, B. J., Jones, C., Jones, L. R., & Van Speybroeck, L. 2007, ApJ, 659, 1125

Mroczkowski, T., et al. 2009, ApJ, 694, 1034

Nagai, D., Kravtsov, A. V., & Vikhlinin, A. 2007, ApJ, 668, 1

Navarro, J. F., Frenk, C. S., & White, S. D. M. 1996, ApJ, 462, 563

Peng, F., & Nagai, D. 2009, ApJ, 693, 839

Sanderson, A. J. R., & Ponman, T. J. 2010, MNRAS, 402, 65

Sanderson, A. J. R., Ponman, T. J., & O'Sullivan, E. 2006, MNRAS, 372, 1496

Sarazin, C. L. 1988, X-ray Emission from Clusters of Galaxies (Cambridge Astrophysics Series; Cambridge: Cambridge Univ. Press)

Shtykovskiy, P., & Gilfanov, M. 2010, MNRAS, 401, 1360

Smith, R. K., Brickhouse, N. S., Liedahl, D. A., & Raymond, J. C. 2001, ApJ, 556, L91

Struble, M. F., & Rood, H. J. 1999, ApJS, 125, 35

Sunyaev, R. A., & Zel'dovich, Y. B. 1972, Comments Astrophys. Space Phys., 4, 173

Suto, Y., Sasaki, S., & Makino, N. 1998, ApJ, 509, 544

Vikhlinin, A., Kravtsov, A., Forman, W., Jones, C., Markevitch, M., Murray, S. S., & Van Speybroeck, L. 2006, ApJ, 640, 691

Vikhlinin, A., Markevitch, M., Murray, S. S., Jones, C., Forman, W., & Van Speybroeck, L. 2005, ApJ, 628, 655

Vikhlinin, A., et al. 2009, ApJ, 692, 1060